Morphing of curved corrugated shells

A.D. Norman, K.A. Seffen* and S.D. Guest

Department of Engineering, University of Cambridge
Trumpington Street, Cambridge CB2 1PZ, UK

October 31, 2008

Abstract

Thin sheet materials of low bending stiffness but high membrane stiffness are often corrugated in order to achieve improvements of several orders of magnitude in bending stiffness with only minimal increases in weight and cost. If these corrugated sheets are initially curved along the corrugations, much of this stiffness gain is lost. In return, the sheets are then capable of significant elastic changes in shape overall, including large changes in overall Gaussian curvature. These shape changes are described here by non-linear and coupled kinematical relationships, which are verified against experiment and finite-element simulations. It is found that gross simplifications can be made about the large displacement behaviour of such shells without a loss of accuracy.

1 Introduction

Corrugated sheets that are also curved along their corrugations can be transformed into a remarkable variety of shapes simply by bending of the surface. Figure 1 shows an example, made by vacuum-forming a sheet of 0.5 mm-thick High-Impact Polystyrene (HIPS). When handled, the shell undergoes dramatic and specific changes in shape, deforming to a tube, a bowl-shape or a saddle-shape in Figs 1b, 1c and 1d respectively.

There are several noteworthy aspects of this deformation. First, the shell accomplishes these significant changes in shape *without* local stretching of the surface: such behaviour is common for thin shell structures, where it is energetically favourable to deform by bending rather than stretching. However, it is clear that an *equivalent* middle surface, or mid-surface, of the corrugations experiences an overall extension, and that this extension also couples to significant extra curving along the corrugations, as shown in Fig. 1b. Ordinary shells do not behave in this manner, nor are they prone to the double bending indicated in Figs 1c and 1d. Depending on the direction of bending across the corrugations, the shell deforms either elliptically, so that the mid-surface acquires positive Gaussian curvature, or hyperbolically into a saddle shape with negative Gaussian curvature. Although not shown, it is difficult to bend the shell back on itself without damage, in the opposite sense to the curved line of corrugations.

This simple structure may not prove attractive for use in traditional engineering structures, which are generally designed to be stiff. But they may usefully serve a new generation of so-called 'morphing' structures that offer both structural integrity and large

---

*Corresponding author. Tel: +44 (0)1223 7 64137 E-mail: kas14@cam.ac.uk

(a) The initial shape, unidirectionally curved along the corrugations.
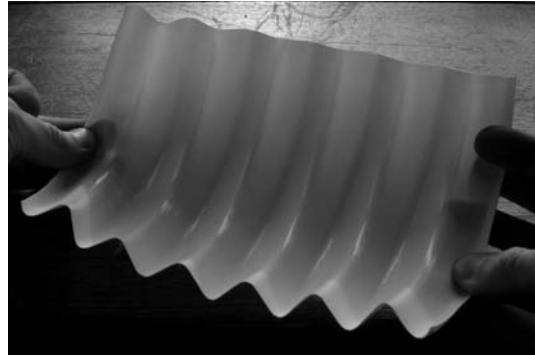
(b) As the curvature increases, so the material expands across the corrugations.

(c) The shell can be inextensibly deformed to a positive Gaussian curvature, (*i.e.* bowl-shaped) *or*

(d) to a negative Gaussian curvature, *i.e.* saddle shaped.

Figure 1: Introducing the curved corrugated forms: these images are all of the same shell, with no significant stretching of the plastic membrane between shapes.

shape-change capabilities. In a previous study [1], we demonstrated that an uncurved corrugated sheet can be made to morph: the corrugations are flattened transversely and the sheet then deforms elastically to a tightly coiled cylinder. Here, the curved corrugated shell affords extra deformation modes, thereby increasing the novelty and range of potential morphing behaviour, which this paper attempts to capture via a compact geometrical model: the prediction of the required forces is the subject of work being performed elsewhere.

The success of our simple model is underpinned by four key assumptions. First, the material is isotropic and remains linear elastic due to the relative thinness of shell despite the large displacements: none of the physical models was ever permanently deformed after severe testing, thus indicating that induced strains were small. Second, the process of handling the open shell without overly constraining the edges leads to natural inextensibility under large displacements. This is not a controversial assumption if the shell is relatively thin and the boundary conditions enable bending to dominate over most of the shell. In practice, an extensible boundary layer must develop near the edge to define the boundary conditions precisely, but the relative thinness of shell and its openness (unlike corrugated fully-closed bellows or Chinese lanterns) ensures that this is a comparatively narrow layer, which does little to affect the *character* of the bulk deformation addressed in this study. The justification of this assumption can be traced to the outcome of a discussion between the earliest pioneers of analytical shell theory: and the interested reader is referred to the "Rayleigh-Love" controversy reported historically by Calladine [2]. Third, local buckling of the shell is neglected on the grounds that we can deform the shell without precipitating local buckling, for example, when bending across the corrugations, the shell can also be stretched in the same direction to eliminate large compressive stresses on the underside. Finally, the overall deformation is described in terms of the performance of the equivalent middle surface. This necessitates a careful consideration of how the inextensible bending of the local shell influences the global deformation mode. Thus, there is a *hierarchy* of deformation, whose analytical relationships are informed by the simplest interpretation of practical behaviour but without being inaccurate, as our theoretical predictions will show.

1.1 Outline of this paper

Section 2 defines our initial system, describing the corrugations and the coordinate systems used to describe them. Section 3 explains how a curved corrugated shell can exhibit shape changes not possible from a 'conventional' uncurved corrugated sheet, and relates their stretching across the corrugations to their curvature. Section 4 tests this coupling relation against measurements of a vacuum-formed plastic shell, and also against a finite-element analysis. This exercise shows an excellent agreement. It validates the assumptions made about the geometric behaviour and paves the way for a full set of compatibility relations in Section 5, which is then compared to a more general behaviour of prototypes in Section 6. Finally, conclusions are drawn in Section 7.

2 Definition of coordinate systems

Figure 2 shows a three-dimensional view of a corrugated shell and a cross-section through a typical corrugation. It has a local right-handed coordinate system with axes x, y and z. Also shown is the equivalent mid-surface, or average surface, of the corrugations, which is defined by the coordinate system of X, Y and Z: note that x and X are both aligned
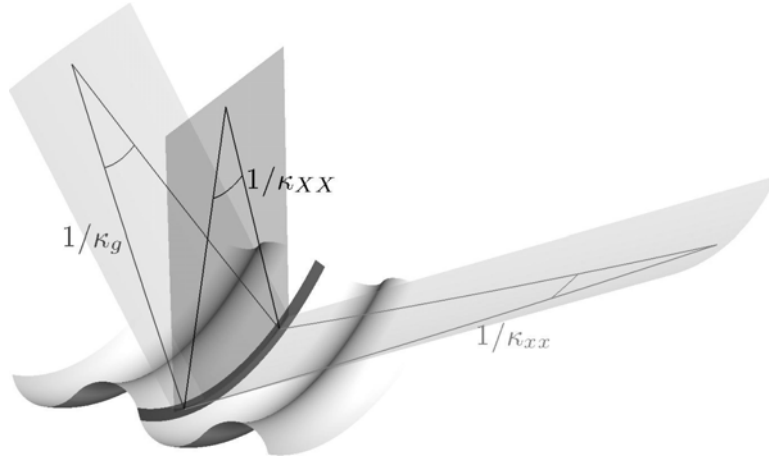
(a) A typical corrugated shell. Looking at a specific strip along the corrugation, shaded black, the strip has some curvature of radius $1/\kappa_{XX}$. This curvature can be split into a component of curvature in the plane of the strip, of radius $1/\kappa_g$, and an out-of-plane component, $1/\kappa_{xx}$.
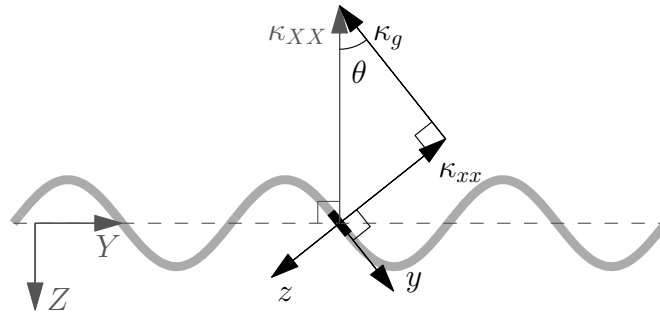
(b) A section through the corrugations, showing the coordinate system used by this paper. (x,y,z) is a local right-handed coordinate system in the shell: (X,Y,Z) is a coordinate system in the equivalent mid-surface, or average surface, of the sheet, shown as a dashed grey line. Both x and X are aligned along the corrugations. The curvatures shown in Fig. 2a are represented by the vectors κ_{XX}, κ_{xx} and κ_g. Each length is the magnitude of the curvature (*i.e.* the inverse of the radius of curvature), and the curvature direction is normal to the tangent of the line and lies in the plane of the curvature.

Figure 2: A typical corrugation, showing the coordinate systems and curvature definitions of this paper. In the X direction, the sheet has an upwards curvature, κ_{XX}. A strip at angle θ to the vertical is shaded black, small in the y direction but running the full length of the sheet in the x direction. κ_{xx} is the out-of-plane curvature of the strip, *i.e.* its shell curvature, while κ_g denotes the *geodesic* curvature of the strip: this is the curvature that the strip's centreline would follow if it were laid on a flat surface. These two curvatures are mutually perpendicular, and are the components of the vector, κ_{XX}.

along the corrugations. The mid-surface has some curvature in the X direction, κ_{XX}, again defined in Fig. 2. The corresponding radius of curvature, $1/\kappa_{XX}$, lies in a vertical plane, and two additional planes are also shown, which contain further radii pertinent to the curving properties of a thin strip running along the shell in the x direction, now described.

The strip is taken to be thin in the y-direction and is inclined to the vertical at an angle θ. The centreline of this strip must, like the mid-surface, have curvature κ_{XX}. The strip's own out-of plane curvature is, however, in another direction, marked by κ_{xx}. The difference between these two is the *geodesic* curvature of the strip, denoted by κ_g: or, if κ_{XX} is shown as a vector, it has orthogonal components of κ_g and κ_{xx}. Note that κ_g is the curvature that the strip centreline would have were the strip removed from the rest of the shell and laid on a flat surface; and this curvature lies in the $x - y$ plane of the shell.

In this paper, it is assumed throughout that the radius of curvature of the shell, $1/\kappa_{XX}$, is much greater than the amplitude of corrugations. Therefore, as the corrugations are considered as a large number of thin strips, all of these strips can be assumed to have exactly the same global curvature κ_{XX}, even though they do not all lie exactly on the mid-surface of the shell.

In addition to the conventional understanding of strain as change in length with regard to the initial length, we consider a property related to strain, but independent of whatever the initial shape of the shell was: referred to as ξ_{YY}, this property is the strain relative to the Y-direction length of the shell when the corrugations are completely flattened out, irrespective of their initial cross-sectional profile. In the terms of Fig. 2, it can be defined as the average value

$$\xi_{YY} = \overline{\left(\frac{\mathrm{d}Y}{\mathrm{d}y}\right)} - 1 \tag{1}$$

where the overbar $\overline{()}$ denotes average. Note that throughout, we assume that all deformations are uniform, that is, independent of location on the shell, which is later shown to be reasonable when compared to observed behaviour.

3   Unidirectional bending behaviour

One purpose of corrugating sheets is to increase their bending stiffness along the corrugations, since such bending must then involve either large stretching and compressive strains in the top and bottom surfaces or total buckling of the corrugations if the cross-sectional shape cannot distort. This section shows that, when the shell edges move freely, the cross-section can undergo transverse bending, which couples to a change in the local and, hence, global curvature along the corrugations. Physically, the local Gaussian curvature must be conserved under the local inextensibility assumption and, thus, a flattening of the cross-section is accompanied by the mid-surface of shell progressively tightening as long as it is initially curved.

Following the definitions in Section 2, we consider a thin x-wise strip of material, at an angle θ to the vertical, with shell curvature, κ_{xx}, and geodesic curvature κ_g. Importantly, κ_{xx} and θ vary as the shell is deformed but κ_g is fixed by the construction and local inextensibility of the shell. The initial shape is shown in perspective view in Fig. 3a. The corrugations are then given a tighter curvature along their corrugations, Fig. 3b, and the overall curvature of the strip, κ_{XX}, has increased. Since κ_g is fixed, so θ increases, *i.e.*
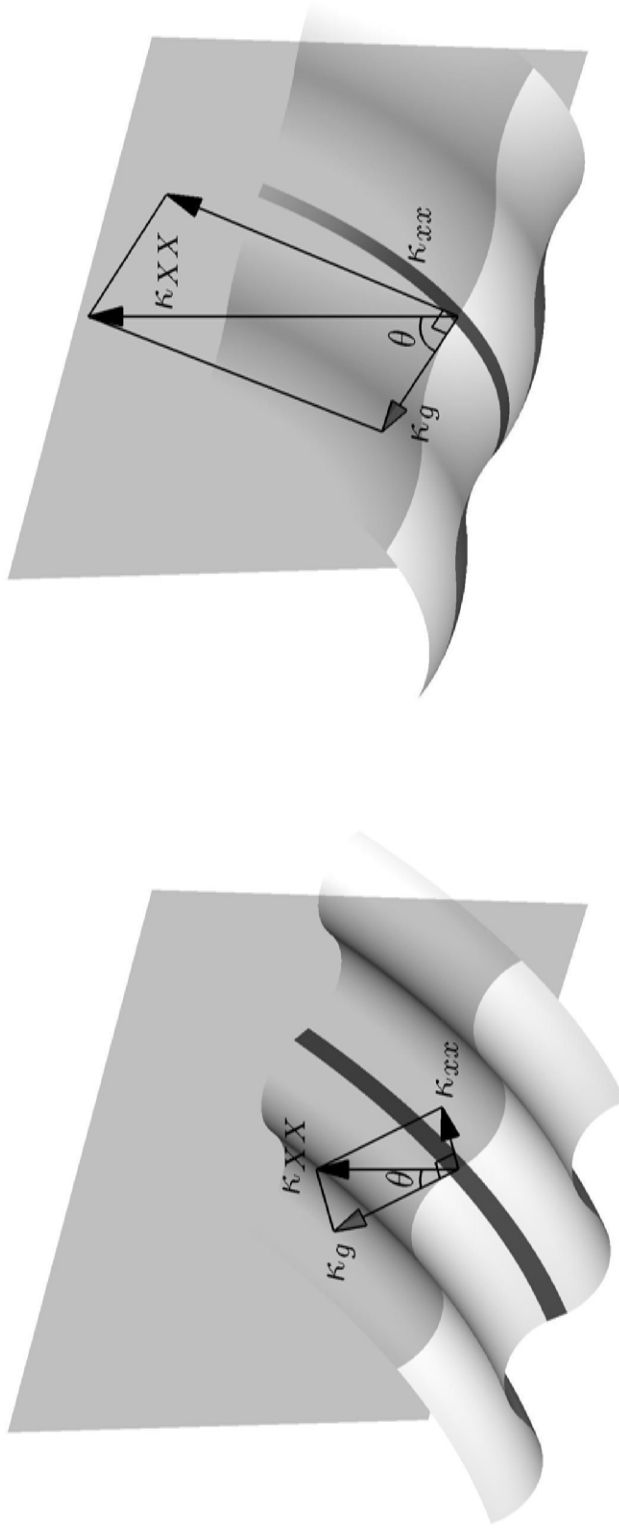
(a) A perspective view of the corrugation profile shown in Fig. 2b. Each thin strip has an out-of-plane curvature κ_{xx} and an in-plane, or geodesic, curvature κ_g, which together make the shell curvature, κ_{XX}, of the equivalent mid-surface of corrugation.

(b) As the sheet is rolled more tightly, κ_{XX} is increased, so θ is increased, since κ_g is fixed by the construction of the shell and the vectors of κ_g and κ_{xx} remain mutually perpendicular.

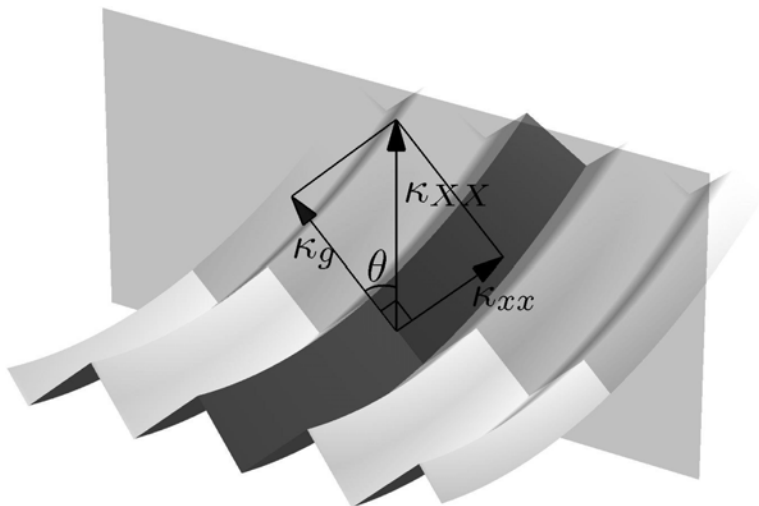**Figure 3:** Unidirectional bending behaviour.

Figure 4: Simplified to the most basic corrugation shape, a triangular wave.

the strip of material rotates so that κ_{xx} increases, maintaining the direction of κ_{XX}. In other words, when the overall curvature of the corrugated sheet, κ_{XX}, is varied, θ and κ_{xx} also vary at a given point of geodesic curvature κ_g according to

$$\kappa_g = \kappa_{XX} \cos\theta \qquad\qquad \kappa_{xx} = \kappa_{XX} \sin\theta \qquad\qquad (2)$$

As these x-wise strips become very narrow in the limit, the shell can be considered as being continuously curved in both the x and y directions, so that the $y - y$ curvature can be defined as

$$\kappa_{yy} = \frac{\partial \theta}{\partial y} \qquad\qquad (3)$$

For a smooth shell, θ and κ_{XX} are initially continuous across the corrugations, and therefore, so is κ_g. If κ_{XX} remains continuous throughout deformation, θ must also remain continuous, and the curvature κ_{yy} always has a finite value. Thus, changes in κ_{XX} are achieved without stretching, but by changes in corrugation curvature, κ_{yy}.

3.1 Unidirectional bending in triangle-wave corrugations

Figure 4 applies the above relations to the simplest corrugation; a sawtooth, or triangle, wave. A single corrugation is created by hinging together at their edges two, initially curved, membrane strips. As before, two additional coordinates, X and Y, lie in the equivalent mid-surface of the corrugated sheet. The stretching and bending of the entire sheet are then easily calculated from:

$$\xi_{YY} = \sin\theta - 1 \qquad\qquad (4)$$
$$\kappa_{XX} = \kappa_g \sec\theta \qquad\qquad (5)$$

where ξ_{YY} refers to the strain relative to the length of the mid-surface when the corrugations are completely flattened out in the Y direction, defined by Eqn 1, and *not* to strain relative to some arbitrary initial shape, as noted before. We define the initial shape to
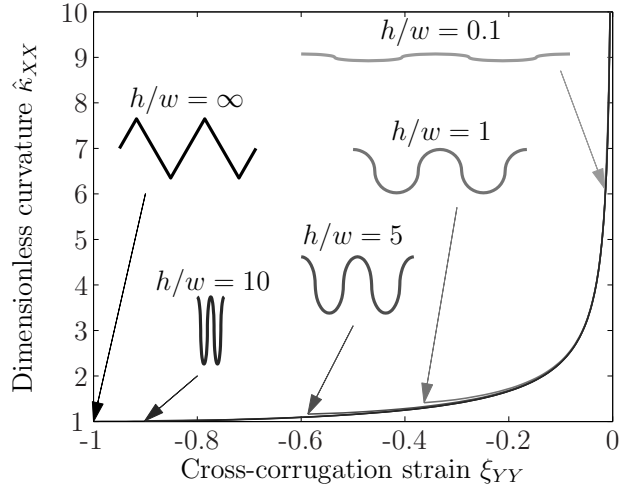
Figure 5: Strain–dimensionless curvature plots for various initially semi-elliptical corrugations (calculated numerically, with each corrugation split into 50 segments) and for a triangular-wave corrugation (calculated analytically). h/w is the ratio of height to width for a quarter corrugation in the locked state: all except the triangular wave are shown in this locked state.

have initial curvature, κ_{XX_0}, and initial strain, ξ_{YY_0}. The relationship between ξ_{YY} and the conventional engineering strain relative to the initial shape is thus:

$$\text{engineering } Y - Y \text{ strain} = \frac{\xi_{YY} - \xi_{YY_0}}{1 + \xi_{YY_0}} \tag{6}$$

It is useful to rearrange Eqns 4 and 5 to eliminate θ, and to give a coupled relationship between the global strain, ξ_{YY}, and curvature, κ_{XX} in terms of the fixed property, κ_g:

$$\xi_{YY} = \sqrt{1 - \left(\frac{\kappa_g}{\kappa_{XX}}\right)^2} - 1 \qquad \text{or} \qquad \kappa_{XX} = \frac{\kappa_g}{\sqrt{1 - (1 + \xi_{YY})^2}} \tag{7}$$

The limits of behaviour become evident from these equations: ξ_{YY} cannot be less than -1, the point at which the corrugations are completely folded up and κ_{XX} reaches its minimum value of $\kappa_{XX} = \kappa_g$; however, ξ_{YY} must always be negative, lies in the range from -1 to zero and κ_{XX} goes to infinity as ξ_{YY} tends towards zero.

3.2 Unidirectional bending in smooth corrugations

The coupled relationships between ξ_{YY} and κ_{XX} in Eqn 7 are straightforward for the given simple sawtooth corrugation: this section compares their performance to the behaviour of those obtained for a more general, smoothly corrugated profile. An equivalent set of closed-form expressions is not possible for a general corrugated profile. Instead, the cross-section must be reduced to a discrete number of curved strips, in order to approximate by numerical solution the resulting change in shape. In the process, the scale of discretisation required for sufficient accuracy presents itself naturally during solution, as will be described.

For any generic corrugation profile, as κ_{XX} is reduced, a length-wise strip of corrugation may rotate sufficiently so that $\theta = 0$. Although over the rest of the corrugation, θ

8

still has some non-zero value, there can be no further increase in κ_{XX} for a fixed κ_g over the strip where $\theta = 0$. Such behaviour defines a lower limit for κ_{XX} without the strain reaching $\xi = -1$: when one part of the corrugation has become completely 'vertical', $\theta = 0$, the shell has 'locked', it cannot flatten any more in the $X - X$ direction, and κ_{XX} has reached a minimum. However, there is no upper limit to κ_{XX}: as the corrugations are completely flattened out, such that θ tends to $\pi/2$, κ_{XX} tends to infinity.

We must now choose some initial corrugation profile to study. Two mathematically expedient forms are a sinusoid and a semi-elliptical profile made of alternating half-ellipses. Because a semi-elliptical profile already has vertical parts, it is therefore locked from the outset whereas a sinusoid is not, and the latter commends itself as a natural initial shape. But a convenient result presents itself, as proven in Appendix A: the locked shape of an initially sinusoidal corrugation is exactly a semi-elliptical corrugation: as a corollary, the same profile initially must, upon reverse deformation where the cross-section is flattened, occupy an exactly sinusoidal profile at some stage later in the deformation. In the process, it is found that the relationship between an initial profile and its locked shape is independent of the initial value of κ_{XX}.

The particular variation of ξ_{YY} with κ_{XX} is found by considering a quarter wave-length of corrugation sub-divided into large number of strips. Each strip has the same κ_{XX}, assuming, as stated in Section 2, that the radius of curvature, $1/\kappa_{XX}$, is much greater than the amplitude of the corrugations. A quarter circle is first divided into discrete segments of equal arc-lengths: these are then shortened in the y direction to form an elliptical profile of the desired aspect ratio, before the actual arc-length, δs, and initial angle, θ_0, of each segment is calculated. From Eqns 2, the final angle θ of each segment is related to the initial curvature, κ_{XX_0}, and final curvature, κ_{XX}, by

$$\cos\theta = \frac{\kappa_g}{\kappa_{XX}} = \frac{\kappa_{XX_0}\cos\theta_0}{\kappa_{XX}} \tag{8}$$

As the angle, θ, of each segment is known, the strain at a given κ_{XX} can be obtained by summing the contribution from strips of width δs:

$$\xi_{YY} = \frac{\sum \sin\theta \delta s}{\sum \delta s} - 1 \tag{9}$$

The above can be re-cast as a continuous integral as follows, performed between limits from $s = 0$ to $s = \lambda$, where λ is the material wavelength of each corrugation, *i.e.* the width of each corrugation when flattened out so that $\xi_{YY} = 0$. The geodesic curvature, κ_g, varies in a known manner across the corrugations such that $\kappa_g = \kappa_g(s)$, and

$$\xi_{YY} = \frac{1}{\lambda}\int_0^\lambda \sin\theta \,\mathrm{d}s - 1 = \frac{1}{\lambda}\int_0^\lambda \sqrt{1 - \left(\frac{\kappa_g(s)}{\kappa_{XX}}\right)^2}\,\mathrm{d}s - 1 \tag{10}$$

While the variation with κ_{XX} of ξ_{YY} becomes known, the performance between different initial shapes must be compared in a meaningful way. A convenient point is at small ξ_{YY}, where the results for all shapes are scaled to match the triangular-wave corrugation, and the corresponding results for curvature are then made dimensionless with respect to the 'locked' curvature of the triangular-wave corrugation. This 'locked' curvature is exactly the geodesic curvature for the triangular-wave corrugation, which we refer to as $\kappa_{g_{\mathrm{Tri}}}$, so that the dimensionless curvature $\hat{\kappa}_{XX}$ is given by
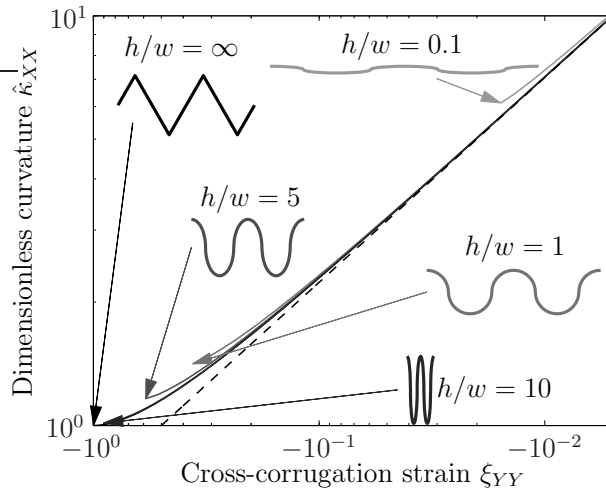
Figure 6: Log-log strain-curvature plots for various corrugations, as in Fig. 5. All terms are as in Fig. 5, but a dashed line has been added representing the equation $2\xi_{YY}\hat{\kappa}_{XX}^2 = -1$, to which all lines tend at large $\hat{\kappa}_{XX}$, which is to say small negative ξ_{YY}.

$$\hat{\kappa}_{XX} = \frac{\kappa_{XX}}{\kappa_{g_{\text{Tri}}}} \tag{11}$$

The dimensionless solutions for a range of semi-elliptical corrugations are shown in Fig. 5.

Figure 5 appears to show a very close correlation between the various shapes, clearly implying that the simple, fully analytical triangular-wave solution remains usefully valid for shapes that are quite different from being a triangular-wave. This is particularly true at high $\hat{\kappa}_{XX}$ and small ξ_{YY}. At larger, more negative ξ_{YY}, the shape curves also appear to be close, but their shallow gradients are deceptive in that, for a given value of $\hat{\kappa}_{XX}$, the variation in ξ_{YY} between curves is of the order of 20 %.

A logarithmic version of this plot is furnished in Fig. 6, and demonstrates that at small strains, the relationship tends to

$$2\xi_{YY}\hat{\kappa}_{XX}^2 = -1 \tag{12}$$

This equation can also be derived from Eqns 4 and 5 by approximating ξ_{YY} to be relatively small.

4   Validation of unidirectional bending models

Equation 10 gives a relationship between strain and curvature that depends upon the fixed shape property of the formed shell $\kappa_g(s)$, which is compared in this section against measurements of a physical prototype and a finite-element analysis.

4.1   Plastic prototype

A prototype shell in plastic was constructed by vacuum forming: Fig. 7 shows the computer-machined mould. The plastic material is High-Impact Polystyrene ('HIPS'), gloss-coated on one side and with an initial nominal thickness of 0.5 mm.
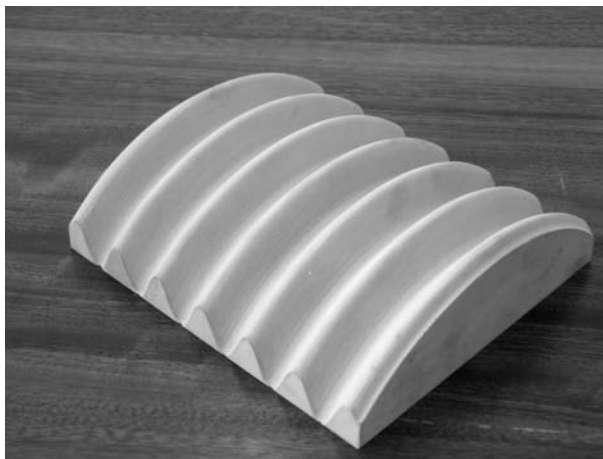
10

Figure 7: The mould used for vacuum-forming the plastic shell. This was produced on a computer-controlled milling machine.

In order to compare its stretching across corrugations, ξ_{YY}, with along-corrugation curvature, κ_{XX}, the shell must be held such that a force in the Y direction is applied without any significant load in the X or Z directions, *despite* the large deflections which accumulate in both those directions as κ_{XX} changes. To enable this, the shell was mounted in an Instron displacement-controlled load testing rig by long wires. When in tension, these wires only transmit force along their own axis. They are fashioned to be as long as the rig allows, so that as the shell coils up, the wire rotates imperceptibly, and the axial force is maintained in the Y direction. Fig. 8 demonstrates that this holds for most of the deformation, being less valid as the corrugations become almost flat where $\xi_{YY} \rightarrow 0$ and κ_{XX} becomes large.

The strain, ξ_{YY}, was calculated by measuring the length of the mid-surface over six corrugations and dividing this by the material length, the latter being found by measuring the width of a flattened thin strip cut from the shell after testing. The curvature, κ_{XX}, was calculated from the chord subtended by the shell in the X direction and its arc length in the same direction, assuming a cylindrical profile. Three separate tests were performed on three separate shells, with the following variations in measurement method:

(i) The Instron's displacement value gave the extension of the shell in the Y direction: a ruler was used to manually measure the chord of the shell in the X direction.

(ii) A digital camera was directed squarely at the shell and photos taken at 2 mm intervals of extension. By manually picking out the coordinates on the image of various points on the corrugations, the changes in lengths could be calculated as ratios of the original lengths, which had been measured by ruler.

(iii) As (i), but a ruler was used to measure the length of the shell in the Y direction, so that there could be no error from the settling of the cables.

Results and discussion are given in Section 4.3.

4.2 Finite element simulation

The analysis was developed to mirror the plastic prototype in terms of its material properties and initial geometry, and was performed using the commercially available software
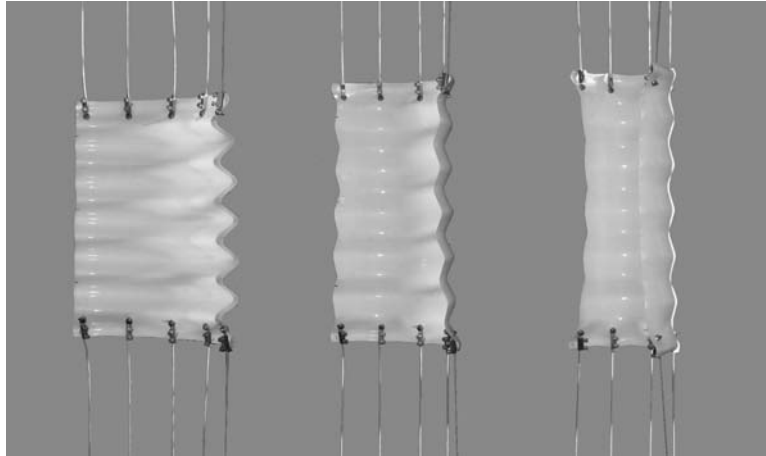
Figure 8: These images show the shell under deformation, at ξ_{YY} values of (left-to-right) -0.25, -0.12 and -0.005. The shell is mounted vertically in a displacement-controlled load-measuring rig, to which it is attached by the wires visible as bright lines on the photographs. These wires are long enough that rotation of the wires remains minimal as the shell deforms, so the forces are approximately purely vertical. In the highly deformed state (right), the wires are no longer transmitting the force perfectly vertically, and κ_{XX} is no longer uniform in the Y-direction of the shell.

package, ABAQUS [3]. A Young's Modulus for the material of 1.47 GPa is given from tests conducted on samples of the material that had been through the vacuum-forming process: these will be significant when constitutive relations for the shell are being produced, but do not matter here. The thickness of the finite element model is taken to be 0.3 mm, while that of the prototype varied from 0.2 mm to 0.4 mm due to the manufacturing process. Again, this variation in thickness affects stiffness relations but not the geometric properties considered here, as long as the assumption that the shell is thin remains valid. A less robust assumption is that of a linearly elastic behaviour. In practice, the elastic modulus softens at high deformations as the HIPS begins to undergo plastic deformation, crazing, and creep, none of which are included in the finite element simulation.

The shell is rendered as a quarter model using four-noded S4F5 shell elements, which interpolate independently the positions of the corner nodes and the normal vector to the shell. A large-displacement, geometrically non-linear static analysis is then performed according to the following boundary conditions. The bottom edge is constrained to move in its own plane, which is a stationary plane: the top surface is likewise constrained in plane, but that plane is then displaced upwards. The right-hand edge is free, as in the experiment, but the left edge is subjected to a symmetric boundary condition, since the shell in the finite-element simulation is one quarter of the experimental shell. There is no need to apply symmetry conditions to the top or bottom edges: they are each constrained to move in their own plane, and the upper plane is then displaced upwards to stretch the shell.

Figure 9 shows the initial and deformed shapes where the global strain and curvature of the middle surface are calculated from a cylinder that is fitted to the computational results, in a similar manner to the physical tests described in the previous section: the vertical displacement of the top edge yields ξ_{YY} and the absolute position of the right-hand edge gives the chord length in order to calculate κ_{XX}.
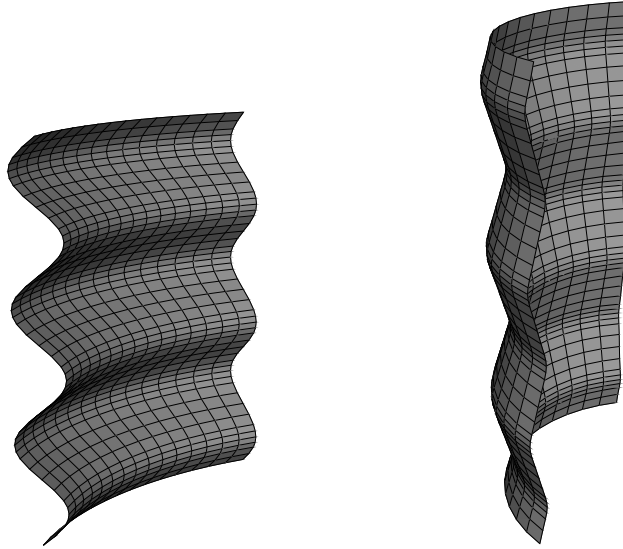
Figure 9: Finite element analysis of the shell. On the left is the initial, unstressed form: on the right, the stressed form. The lower edge was constrained not to move out of its plane, but movement within its plane was free. The left-hand edge had a symmetry constraint. The upper edge had an upwards displacement rate applied to it, but was unconstrained in other directions.

4.3   Results and discussion

Figure 10 presents the analytical results following the numerical integration method described in Section 3.2, the finite element analysis output and the measurements from the physical experiment. In addition, it presents the result for a triangular-wave corrugation, which has the very simple closed-form expression given in Equation 7. This requires the selection of a suitable value of κ_g for the triangular-wave corrugation: the value was chosen so that the curve met the experimental and FE results at the initial state, *i.e.* the lowest ξ_{YY}. Owing to this matching of the initial conditions, it was more sensible to plot the conventional engineering strain of the shell relative to its initial state, rather than the strain, ξ_{YY}, of mid-surface length to the material length in the corrugations: recall that the relation between ξ_{YY} and the engineering strain is given in Eqn 6.

The correlation between these results is very good, such that it is hard to distinguish the results, even for the triangular-wave model. At larger deformations, the plastic shells deform a little more than expected due to the stretching and possible creeping of the plastic shell. It can be concluded therefore that the assumptions hold well, namely, that:

(i) the local shell deforms purely in bending: stretching in the material is not significant, as demonstrated by the correlation between the geometric analytical model and the finite element simulation;

(ii) nonlinearities in the material are not significant, as shown by the correlation between the finite element simulation and experiment;

(iii) the radius of curvature $1/\kappa_{XX}$ is sufficiently much greater than the amplitude of corrugations; and

(iv) the relationship between cross-corrugation strain and along-corrugation curvature of an initially triangular-wave corrugation is only negligibly different from that of a sinusoidal corrugation.
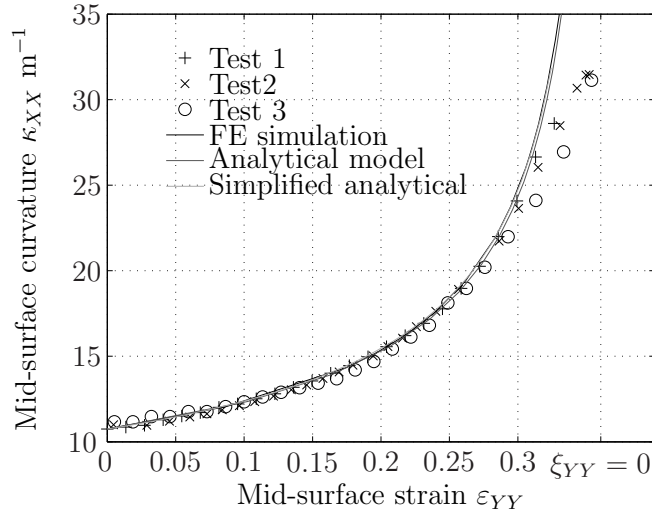
Figure 10: Plot of mid-surface curvature κ_{XX} in m^{-1} against mid-surface engineering strain, Eqn 6. The experiment began at the initial strain and curvature shown at the leftmost edge of the curves, in which state the shell was unstressed. The finite-element simulation and both analytical models took this as their initial point. The FE analysis and the 'exact' analytical expressions began from a sinusoidal shape at this point, which matched the plastic shell tested: the simplified model assumed a triangular-wave corrugation. The tailing-off of the experiment at high κ_{XX} corresponds to stretching of the plastic shell.

In addition, the results validate the methodological assumption in Section 4.1 that the long wires do not rotate sufficiently to change the direction of axial force in the wires acting on the sheet, except at very high values of κ_{XX}.

5 Bidirectional bending

The uni-directional bending in the previous section enabled validation of the coupling relationship between κ_{XX} and ξ_{YY}, originally proposed in Section 3. As noted in Section 1, the shell can be deformed so that the mid-surface of the corrugated shell becomes doubly curved. In this section, we aim to qualify this behaviour by introducing κ_{YY}, the cross-wise curvature of the same mid-surface alongside κ_{XX} so that changes in its Gaussian curvature, K, can be quantified using a well-known compatibility statement; moreover, we formally calculate κ_{YY} assuming that K is prescribed in advance, to confirm results using physical models. Since this section is concerned with physically compatible shape-change rather than with stiffness, certain stretching/bending strains can be defined to be free with effectively zero stiffness and others to be fixed with infinite stiffness; and, for the initial discussion, we need to refer to conventional engineering strain, denoted by ε.

Since stretching in the X direction or X-Y shear must involve stretching of the membrane, $\varepsilon_{XX} = \varepsilon_{XY} = 0$. In the Y direction, the corrugations can flatten out and cause the homogenised mid-surface to stretch, so ε_{YY} is free. The curvatures, κ_{YY} and κ_{XY}, are also free; κ_{XX} is free but, as noted above in Section 3, it is coupled to the transverse strain, where both are generally a function of θ and κ_g, as in Eqn 10. However, nothing has been said about their relationship to the cross-wise curvature, κ_{YY}, and it is necessary to introduce one simplifying assumption, namely: *the relation between ξ_{YY} and κ_{XX} is*

14

independent of the variation of κ_{YY}. This is valid if κ_{YY} has a negligible effect on the corrugation profile, *i.e.* if the radius of curvature $1/\kappa_{YY}$ is significantly greater than the amplitude of the corrugations, as per κ_{XX}.

The Gaussian curvature, K, of a shell is the product of the two principal curvatures κ_1 and κ_2, and is equal to the solid angle subtended per unit area of the shell. It can also be defined from the local membrane strains and their spatial rates of change. Calladine ([4] pp.154) derives this relationship for small strains; large strains affect the area over which solid angle is measured, and his equation, when appropriately modified for large strains (*e.g.* see pp.178), becomes

$$K = \left[2\frac{\partial^2\varepsilon_{XY}}{\partial X \partial Y} - \frac{\partial^2\varepsilon_{XX}}{\partial Y^2} - \frac{\partial^2\varepsilon_{YY}}{\partial X^2}\right](1+\varepsilon_{XX})^{-1}(1+\varepsilon_{YY})^{-1} \tag{13}$$

Several of these terms have already been defined to be zero, and replacing ε_{YY} with ξ_{YY} via Eqn 6, then

$$K = -\frac{\partial^2\xi_{YY}}{\partial X^2}(1+\xi_{YY})^{-1} \tag{14}$$

From Eqn 4, ξ_{YY} and its derivatives are

$$\xi_{YY} = \sin\theta - 1 \qquad \frac{\partial\xi_{YY}}{\partial X} = \frac{\partial\theta}{\partial X}\cos\theta \qquad \frac{\partial^2\xi_{YY}}{\mathrm{d}X^2} = \frac{\partial^2\theta}{\partial X^2}\cos\theta - \left(\frac{\partial\theta}{\partial X}\right)^2\sin\theta \tag{15}$$

and substituting these into Eqn 14,

$$K = \left(\frac{\partial\theta}{\partial X}\right)^2 - \frac{\partial^2\theta}{\partial X^2}\cot\theta \tag{16}$$

Here, for simplicity, shells with no twist are considered, so that $\kappa_{XY} = 0$; the principal curvatures are κ_{XX} and κ_{YY}, such that

$$K = \kappa_{XX}\kappa_{YY} \tag{17}$$

$$\therefore \qquad \kappa_{YY} = \kappa_g^{-1}\cot\theta\left[\left(\frac{\partial\theta}{\partial X}\right)^2 - \frac{\partial^2\theta}{\partial X^2}\cot\theta\right] \tag{18}$$

All other bending and stretching strains are zero. Thus, the shape of mid-surface is defined, beginning with $\kappa_g(\mathrm{X},\mathrm{Y})$ and $\theta(\mathrm{X},\mathrm{Y})$. Note that κ_g is a physical property of the model, so that shape change comes through manipulation of θ.

# 6   Validation of models of bidirectional bending

This section uses the model of the equivalent mid-surface and compares its results, in a crude fashion, to paper models. These paper models use triangular corrugations for they are simple to make and their average geodesic curvature is constant over the whole shell, equal to 3.5 m^{-1} and equivalent to a radius of 28 cm. These paper shells have a square planform of 0.3 m by 0.3 m.
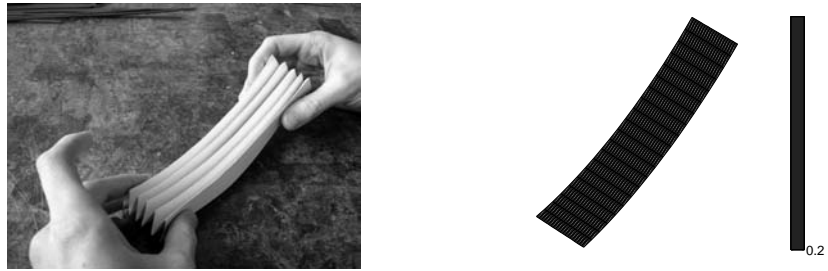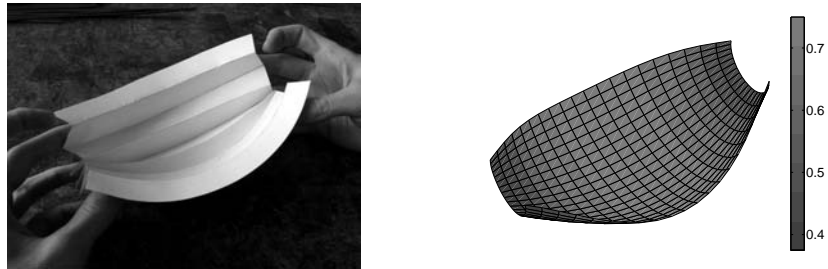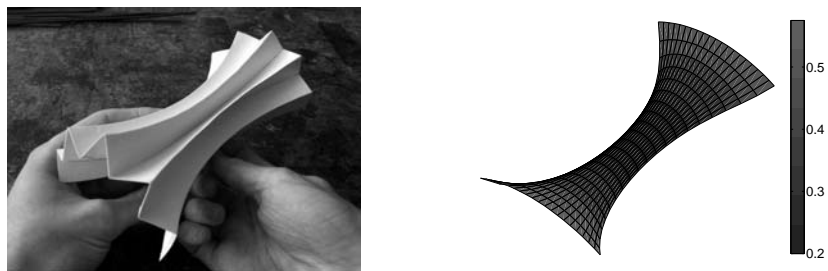
(a) Tightly folded: $a_0 = 0.2$, $a_1 = 0$, $a_2 = 0$
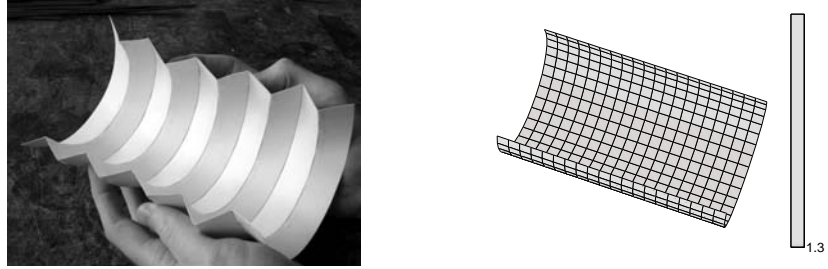
(b) Opened: $a_0 = 1.3$, $a_1 = 0$, $a_2 = 0$
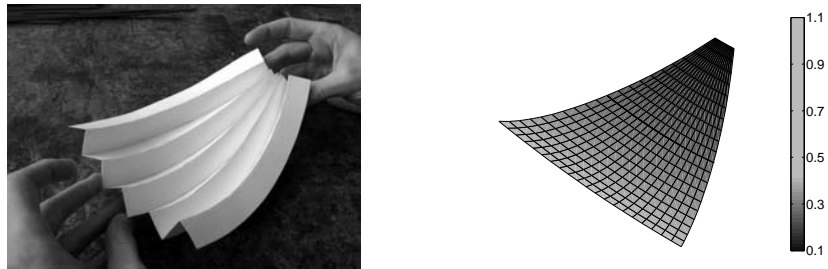
(c) Linearly varying θ: $a_0 = 0.6$, $a_1 = 1$, $a_2 = 0$

(d) Positive K: $a_0 = 0.75$, $a_1 = 0$, $a_2 = -1.5$

(e) Negative K: $a_0 = 0.2$, $a_1 = 0$, $a_2 = 1.5$

Figure 11: Comparison of the physical model (left) to the analytical model (right) with quadratic variation of θ with X, with coefficients a_n as described by Eqn 19. These coefficients were chosen by trial and error to match the observed behaviour. They have been made dimensionless with respect to the length of the shell. On the computer plots, colour denotes the angle θ in radians, as per the colourbars on the right.

The simplest variation in θ to produce interesting results is a polynomial of order n in the X direction; by not varying in the Y direction, the triangular corrugations are uniformly compressed, or expanded, along a given transverse line during deformation:

$$\theta = \sum_{n=0}^{m} a_n X^n = a_m X^m + a_{m-1} X^{m-1} + \ldots + a_2 X^2 + a_1 X + a_0 \tag{19}$$

Figure 11 compares the physical models and this mathematical model, using a polynomial for θ of order 2 or less, *i.e.* $a_n = 0$ for $n > 2$. In other words, this shell has the shape properties

$$\theta = a_2 X^2 + a_1 X + a_0 \tag{20}$$
$$K = (2a_2 X + a_1)^2 - 2a_2 \cot \theta \tag{21}$$

θ must lie in the range $0 \leq \theta \leq \pi/2$, so $\cot \theta$ is always positive. So, if θ varies linearly ($a_2 = 0$, Fig. 11c), its Gaussian curvature, K, must be positive, but a positive a_2 can give negative K.

In Fig. 11, these equations are used to describe the shape change of a simulated mid-surface, which is compared to the paper shell. Values of a_n have been chosen by trial and error such that the surfaces from the simulation match as closely as possible the mid-surfaces of the shell when photographed in various configurations. Nonetheless, the agreement is very good despite the limited specification of θ, and the essential behaviour is captured.

7   Conclusions

It is generally known that a shell structure cannot undergo a change in Gaussian curvature without significant stretching. In this study, it has been shown that a corrugated shell with some initial curvature across the corrugations can experience very large changes in the Gaussian curvature and shape of its mid-surface without local stretching. Such behaviour may prove useful in the design of novel morphing surfaces, for it extends the range of kinematical performance to that not obtained with conventional shells. The shape change of shells of any complexity can be described using the compact analytical model presented in Section 5, which assumes that the relation between ξ_{YY} and κ_{XX} is independent of the variation of κ_{YY}. It has also been shown that a simpler triangular wave corrugation can provide a reasonably accurate description of the geometric behaviour of shells of a continuous corrugation wave. The next step in this work is a study of the structural mechanics of these shells, and this is the subject of ongoing work by the authors.

References

[1] Norman, A. D., Seffen, K. A., and Guest, S. D. Multistable corrugated shells. *Proceedings of the Royal Society, London, A 464*, 2095 (July 2008), 1653–1672.

[2] Calladine, C. R. Love centenary lecture: the theory of thin shell structures 1888-1988. *Proceedings of the Institution of Mechanical Engineers 202*, 42 (1988).

[3] Hibbitt, Karlsson, and Sorenson. *ABAQUS Version 6.7*. Hibbitt, Karlsson & Sorenson, Inc., Pawtucket, 2008.

[4] Calladine, C. R. *Theory of Shell Structures*. Cambridge University Press, 1983. ISBN 0521238358.

[5] Abramowitz, M., and Stegun, I. A. *Handbook of Mathematical Functions with Formulas, Graphs, and Mathematical Tables*, 9th ed. Dover, New York, 1972. Chapter 17.

A   Locking of sinusoidal corrugations

This section demonstrates that, when a sinusoidally-corrugated sheet curved along its corrugations 'locks' in the fashion shown in Section 3, the corrugations adopt an exactly semi-elliptic shape. In other words, a sinusoidally-corrugated shell and a shell with semi-elliptic corrugations are *the same shell*, in a different state of inextensional deformation.

Consider a generic sinusoidal corrugation of trough-to-peak amplitude, A, and wavelength, Λ, as shown in Fig. 12a. A particular element of material is located at a distance, s, along the material path of the corrugation from the origin, at coordinates (Y,Z), and making an angle Ψ to the Y-axis. It then deforms to the locked situation in Fig. 12b. The same element is now at position (y,z), making an angle ψ to the y-axis. Since the material is assumed not to stretch, s remains unchanged. This section will assume that the locked shape is elliptical, and then prove this to be so.

The initial, sinusoidal, corrugation is described in Y-Z space as

$$Z = \frac{1}{2}A\left(1 - \cos\frac{2\pi Y}{\Lambda}\right) \tag{22}$$

where Ψ is given by

$$\tan\Psi = \frac{\mathrm{d}Z}{\mathrm{d}Y} = \frac{A\pi}{\Lambda}\sin\frac{2\pi Y}{\Lambda} \tag{23}$$

The path length, s, along the corrugations from the origin to this point (Y,Z) is the integral

$$s = \int_0^Y \sqrt{1 + \left(\frac{\mathrm{d}Z}{\mathrm{d}Y}\right)^2}\,\mathrm{d}Y \tag{24}$$

$$= \int_0^Y \sqrt{1 + \left(\frac{A\pi}{\Lambda}\sin\frac{2\pi Y}{\Lambda}\right)^2}\,\mathrm{d}Y \tag{25}$$

$$= \frac{\Lambda}{2\pi}\mathrm{E}\left(\frac{2\pi Y}{\Lambda}\,\middle|\,-\left[\frac{\pi A}{\Lambda}\right]^2\right) \tag{26}$$

where $\mathrm{E}(\phi|m)$ is an incomplete elliptic integral of the second kind [5].

The next step is to find the 'locked' shape: the final angle, ψ, can be determined from the *initial* position (Y,Z). Recall from Section 3 that for any specific material point, $\kappa\sin\psi$ is constant, see Eqn 2). The curvature along the corrugations is uniform over the
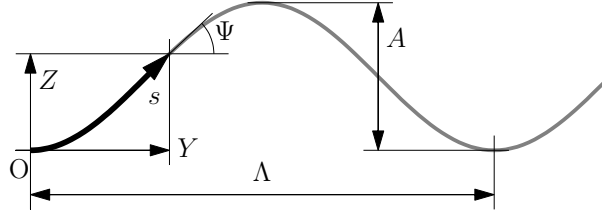
(a) The corrugations in their initial sinusoidal configuration, with amplitude A and wavelength Λ.
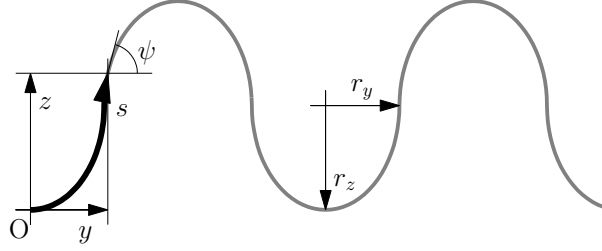
(b) The same corrugations, to the same scale, when deformed to their 'locked' configuration.

Figure 12: An initially sinusoidal corrugation (12a) and its 'locked' shape (12b). This appendix proves that the latter shape is composed of half-ellipses, of radii r_y and r_z.

shell at any specific point in time. Therefore, the ratio at any specific material point between the initial curvature and final curvature is uniform over the whole shell, and so the ratio between $\sin\Psi$ and $\sin\psi$ is, likewise, uniform over the whole shell. The curvature change at 'lock' is controlled by the curvature change at the steepest point, where ψ goes to 90 ° and $\sin\psi$ goes to 1. The ratio at any point between $\sin\psi$ and $\sin\Psi$ is simply the maximum value of $\sin\Psi$, which occurs at $2\pi Y/\Lambda = \pi/2$, so that

$$\sin\psi = \frac{\sin\Psi}{\max(\sin\Psi)} \tag{27}$$

Using the general identities that

$$\sin\theta \equiv \frac{\tan\theta}{\sqrt{1+\tan^2\theta}} \qquad\qquad \tan\theta \equiv \frac{\sin\theta}{\sqrt{1-\sin^2\theta}} \tag{28}$$

it is found that

$$\sin\psi = \frac{\frac{\frac{A\pi}{\Lambda}\sin\frac{2\pi Y}{\Lambda}}{\sqrt{1+\left(\frac{A\pi}{\Lambda}\sin\frac{2\pi Y}{\Lambda}\right)^2}}}{\frac{\frac{A\pi}{\Lambda}}{\sqrt{1+\left(\frac{A\pi}{\Lambda}\right)^2}}} = \frac{\sqrt{1+\left(\frac{A\pi}{\Lambda}\right)^2}\sin\frac{2\pi Y}{\Lambda}}{\sqrt{1+\left(\frac{A\pi}{\Lambda}\sin\frac{2\pi Y}{\Lambda}\right)^2}} \tag{29}$$

leading to an expression for the locked angle ψ,

$$\tan\psi = \frac{\sqrt{1+\left(\frac{A\pi}{\Lambda}\right)^2}\sin\frac{2\pi Y}{\Lambda}}{\sqrt{1+\sin^2\frac{2\pi Y}{\Lambda}}} \tag{30}$$

An interesting result is that the locked shape is a function of the initial shape only, and is independent of the initial X-X curvatures, κ_{xx} and κ_g.

To verify that this coincides with an elliptical corrugation, it is necessary to find ψ in terms of the material's final position (y,z). The first quarter-corrugation of a generic corrugation is defined by the equation below, in terms of y and z and with the material having rotated to angles ψ:

$$\left(1 - \frac{z}{r_z}\right)^2 + \left(\frac{y}{r_y}\right)^2 = 1 \tag{31}$$

$$\tan\psi = \frac{\mathrm{d}z}{\mathrm{d}y} = \frac{\frac{r_z}{r_y} \cdot \frac{y}{r_y}}{\sqrt{1 - \left(\frac{y}{r_y}\right)^2}} \tag{32}$$

where r_y and r_z are the horizontal and vertical radii of the ellipse, as shown in Fig. 12b. The arc length s is, again, the integral over

$$s = \int_0^y \sqrt{1 + \left(\frac{\mathrm{d}z}{\mathrm{d}y}\right)^2}\,\mathrm{d}y \tag{33}$$

$$= \int_0^y \sqrt{1 + \frac{\left(\frac{r_z}{r_y} \cdot \frac{y}{r_y}\right)^2}{1 - \left(\frac{y}{r_y}\right)^2}}\,\mathrm{d}y \tag{34}$$

$$= r_y \mathrm{E}\left(\arcsin\frac{y}{r_y}\Bigg|1 - \left[\frac{r_z}{r_y}\right]^2\right) \tag{35}$$

In order to demonstrate that this is the locked shape of the sinusoidal corrugations, values of r_y and r_z are found such that Eqns 30 and 26 are equivalent to Eqns 32 and 35 respectively. This occurs when

$$r_y = \frac{\Lambda}{2\pi} \qquad\qquad \left(\frac{A}{2}\right)^2 r_z = \frac{A}{2}\sqrt{1 + \left(\frac{\Lambda}{A\pi}\right)^2} \tag{36}$$

with a relationship between the initial and final positions

$$y = \frac{\Lambda}{2\pi}\sin\frac{2\pi Y}{\Lambda} \qquad\qquad z = Z\sqrt{1 + \left(\frac{\Lambda}{A\pi}\right)^2} \tag{37}$$

Thus, a sinusoidal corrugation has been shown to lock to an elliptical corrugation. Likewise, starting with an elliptically corrugated sheet that is curved in the X direction, which is then coiled up in the X direction, the corrugation profile will deform, and will, at one unique instant, take an exactly sinusoidal profile.